

Arresting of interfacial phase separation with an imposed flow

Ryuta X. Suzuki ^{1,2,*}, Shoji Seya,¹ Takahiko Ban ³, Manoranjan Mishra ⁴,
and Yuichiro Nagatsu ¹

¹*Department of Chemical Engineering, Tokyo University of Agriculture and Technology, Naka-cho 2-24-16, Koganei, Tokyo 184-8588, Japan*

²*PRESTO, Japan Science and Technology Agency, Kawaguchi, Saitama 332-0012, Japan*

³*Division of Chemical Engineering, Department of Materials Engineering Science, Graduate School of Engineering Science, Osaka University, Machikaneyamacho 1-3, Toyonaka City, Osaka 560-8531, Japan*

⁴*Department of Mathematics, Indian Institute of Technology Ropar, Rupnagar 140001, India*



(Received 16 August 2022; accepted 5 January 2024; published 14 February 2024)

Using fluid displacement in a Hele-Shaw cell, we experimentally demonstrate the arresting effect of an imposed flow on a phase separation occurring in a growing liquid-liquid interfacial region, unlike in an initially homogeneous single-phase mixture quenched within the miscibility gap. Increasing the imposed flow rate reduces the exponent α in the form $\Delta A \propto t^\alpha$, where ΔA is the increase in the area occupied by the displacing fluid owing to phase separation. We show that α can be expressed as a function of the ratio of the phase separation rate to the flow rate on a single curve, indicating that the competition between the imposed flow and phase separation rates determines the degree of the interfacial phase separation. The arresting effect and the mechanism are verified by a numerical simulation.

DOI: [10.1103/PhysRevFluids.9.024003](https://doi.org/10.1103/PhysRevFluids.9.024003)

I. INTRODUCTION

Phase separation is a phenomenon wherein a mixed solution separates into two phases; it has received significant attention because of its wide applications in biology, biochemistry, physics, etc. There are two types of phase separation: nucleation [1] and spinodal decomposition [2]. Spinodal decomposition is the process by which a thermodynamically unstable mixture separates into two phases without nucleation. In a binary mixture, when the second derivative of the free energy with respect to composition is negative, spinodal decomposition occurs. The signature feature of phase separation is coarsening, in which the characteristic length scale of phase separation L grows in time according to a power law, $L(t) \propto t^\alpha$, where α is an exponent that depends on the growth mechanism. Such thermodynamic coarsening was studied in the context of solid alloys [3]. For example, in the Ostwald ripening process, one of the thermodynamic coarsening processes in solid alloys wherein large phase domains grow at the expense of smaller ones, the domain length (here, the radius of a droplet) increases by $t^{1/3}$ [4]. This was proven by the Lifshitz-Slyozov-Wagner theory [5,6]. Thermodynamic coarsening can be fundamentally altered in fluid mixtures by means of hydrodynamic effects that lead to a different algebraic growth of the domain. For instance, Siggia [2] demonstrated that hydrodynamics accelerated the domain growth where a length scale, e.g., the radius of the droplet, of spinodal decomposition increased linearly with time (proportional to t^1).

The thermodynamic coarsening dynamics of phase separation in fluid mixtures have been reported to be modified by imposed flows, such as a simple shear flow, turbulent flow, and chaotic flow. For a simple shear flow, a highly anisotropic layered phase ordering in mixtures has been reported

*Corresponding author: ryuta.x.suzuki@gmail.com

through experiments and numerical simulations [7–11]. Using light scattering experiments, early experimental studies [12,13] showed that a turbulent flow suppressed the spinodal decomposition-type phase separation of a binary mixture. The suppression or arrest of spinodal decomposition by a turbulent flow has also been substantiated by numerical studies [14–16]. Numerical studies have investigated the time evolution of the characteristic length of the fluid domain. Although the length increases with time according to a power law, $L(t) \propto t^\alpha$ in the absence of turbulence, this increase is arrested by turbulent flow as the system attains a steady state. For a chaotic flow, coarsening arrest has been validated numerically [17]. Recently, a computational study of the arrest of thermodynamic coarsening in a fluid mixture by other types of imposed flow was conducted by Fu *et al.* [18]. In their research, the separating phase exhibited a large viscosity contrast; thus, a periodic left-to-right flow imposed caused a hydrodynamic instability due to the viscosity contrast, i.e., viscous fingering (VF) [19], which shows a fingerlike interface when a less-viscous fluid displaces a more viscous one in porous media. The coarsening arrest by VF was observed numerically, along with the attainment of a statistical steady state by the system, in which the binary mixture was always driven far from equilibrium.

In all the aforementioned studies that investigated the coupling between phase separation and imposed flows, the mixture solution was premixed. Particularly in the experiments, the mixture was initially prepared to achieve a homogeneous phase in the stable region of the phase diagram. Subsequently, when the temperature was typically reduced below a critical temperature, phase separation began to occur. However, our research group recently performed an experimental study on a different type of coupling between phase separation and an imposed flow [20]. The study is VF with phase separation. In this experiment, when a less-viscous solution, which is not premixed with a more-viscous one, displaces the more-viscous one in a Hele-Shaw cell (which is a thin gap between two parallel plates), phase separation occurs only in the vicinity of the growing interface, which forms a fingerlike configuration. The occurrence of the interfacial phase separation was verified by calculating the second derivative of the free energy of mixing with respect to the concentration of one chemical species. It is known that spontaneous convection occurs in the interfacial region between two liquids where spinodal decomposition occurs due to body forces originating from the chemical potential gradient (Korteweg force) [21–26]. Suzuki *et al.* (2020) [20] explained that the nature of phase separation and spontaneous convection caused viscous fingers to pinch off and droplets to detach from the mother fingers. The detached droplets self-propelled in arbitrary directions owing to spontaneous convection. In this study, the occurrence of spinodal decomposition-type phase separation in the fluid displacement was experimentally verified through area measurement of the less viscous liquid. An increase was observed in the pattern area due to spinodal decomposition, compared to that in the corresponding immiscible case; this increase, denoted as $\Delta A(t)$, grew with time according to a power law, $\Delta A(t) \propto t^\alpha$. It was found that $\alpha = 1.7$ when the multiple droplet pattern was observed most remarkably. That $\Delta A \propto t^{1.7}$ in area scales implies that $l(t) \propto t^{1.7/2} = t^{0.85}$ in length scales. This was close to a linear evolution with time (t^1 dynamics). These results indicate that the area increase is convection driven; therefore, spontaneous convection plays a dominant role, and this should be considered proof of occurrence of a spinodal-type phase separation. Subsequently, our group has succeeded in numerical reproduction of such topological change of VF interface by establishing a mathematical model that combines phase separation effect and Korteweg force with VF hydrodynamics [27].

In this context, it is important to determine the effects of the imposed flow on the properties of such type of phase separation that occurs in a growing liquid-liquid interfacial region. Several questions arise: How does the imposed flow impact the properties of the this type of phase separation? Is the interfacial phase separation enhanced or suppressed as the imposed flow rate increases? To address these questions, in this study, we perform the above-mentioned fluid displacement experiment, which involves spinodal decomposition-type phase separation by changing the flow rate; we analyze the properties of the interfacial phase separation through area measurement. Herein, we demonstrate that the interfacial phase separation is arrested with an increase in the flow rate. We claim that the outcome of the present study is an instance of an imposed flow arresting the phase

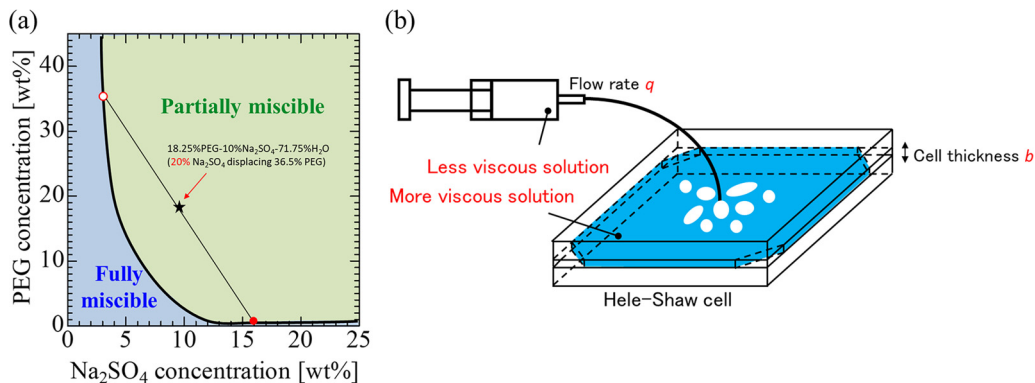


FIG. 1. (a) Phase diagram of PEG, Na_2SO_4 , and water system, and (b) the fluid displacement apparatus.

separation occurring in a growing liquid-liquid interfacial region; this is a different type of phase separation arrest from those previously reported. In addition, we demonstrate that the competition between the imposed flow and phase separation rates determines the degree of the interfacial phase separation and that the arrest mechanism is different from that in phase separations occurring in the bulk. The above experimental results and proposed mechanism are verified by numerical simulation.

II. EXPERIMENT

For the liquid system, we employed an aqueous two-phase system (ATPS) comprising polyethylene glycol (PEG) (average molecular weight $M_w = 8000$), sodium sulfate (Na_2SO_4), and water. The phase diagram of PEG, sodium sulfate, and water is shown in Fig. 1(a) [28]. In a previous report [20], a combination of 36.5 wt % PEG solution as a more viscous displaced liquid and 20 wt % Na_2SO_4 solution as a less viscous displacing liquid was confirmed to cause spinodal-type phase separation at the liquid-liquid interfacial region, based on the second derivative of the Gibbs free energy. Therefore, these compositions were used in the present study. The concentration of the interface of 36.5 wt % PEG and 20 wt % Na_2SO_4 solutions is shown as a star point in Fig. 1(a). This solution goes to separate into a PEG-rich phase (phase L, lighter phase; Na_2SO_4 and PEG concentrations are 3.2 and 36.5 wt %, respectively; red open circle) and a salt-rich phase (phase H, heavier phase; Na_2SO_4 and PEG concentrations are 16.0 and 1.4 wt %, respectively; red solid circle). The density and viscosity of the 36.5 wt % PEG solution were 1070 kg/m^3 and 112 mPa s , respectively, whereas those of the 20 wt % Na_2SO_4 solution were 1190 kg/m^3 and 2.08 mPa s , respectively. The fluid displacement apparatus was the same as that used in a previous study [20], which is shown in Fig. 1(b). The more viscous PEG solution was dyed blue using indigo carmine for visualization of the displacement pattern. The displacement of a more viscous fluid by a less viscous fluid was performed using a Hele-Shaw cell in a radial geometry, wherein the pattern develops in a radial direction owing to fluid injection from a point. The gap width b was set as 0.3 mm . The injection flow rate q was varied between 6.70 and $33.5 \text{ cm}^3/\text{h}$.

The degree of the interfacial phase separation in the displacement was investigated by measuring the increase in area due to the phase separation; to determine this increase, the area calculated from the injection volume was subtracted from the measured area of the injected 20 wt % Na_2SO_4 solution. The images of the displacement pattern were binarized at a threshold of the color level, and the area measurement was performed using the binarized image. Both procedures were conducted using the free software IMAGEJ.

We define the characteristic time of the flow as the nominal residence time in the Hele-Shaw cell: $\tau_f = \pi b R_{\text{HS}}^2 / q$, where R_{HS} is the radius of the circular measurement region, which is 58 mm (Fig. 2). We use τ_f as a parameter representing the flow rate effects, wherein τ_f is inversely proportional to q (τ_f decreases with an increase in q). Figure 2 shows the time evolution of the displacement patterns.

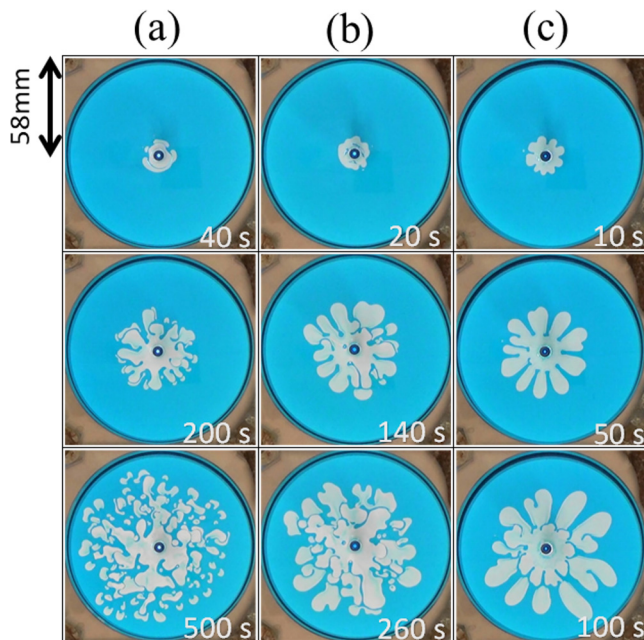


FIG. 2. Time evolution of displacement patterns at (a) $\tau_f = 1.70 \times 10^3$ s, (b) $\tau_f = 8.52 \times 10^2$ s, and (c) $\tau_f = 3.41 \times 10^2$ s.

The liquid-liquid interface grows radially and deforms into fingering or droplets gradually over time. For high τ_f (low q), in Fig. 2(a), for $\tau_f = 1.70 \times 10^3$ s, some droplets were created at the early stage, and the number of droplets increased with time. Meanwhile, for low τ_f (high q), in Fig. 2(c), for $\tau_f = 3.40 \times 10^2$ s, no droplet was observable at the early stage; however, some large droplets detached from the mother fingers at the later stage. In Fig. 2(b), for $\tau_f = 8.52 \times 10^2$ s, we observed intermediate behavior, i.e., some droplets were created at the middle stage, and the number of droplets in the later stage was less than that for $\tau_f = 1.70 \times 10^3$ s [Fig. 2(a)]. Movies depicting the temporal pattern evolution for various τ_f values are provided in the Supplemental Material [29]. This qualitative visual evidence suggests that an increase in the flow rate arrests the interfacial phase separation because of the formation of the droplets caused by the phase separation [20].

The time evolution of the area measurements for various τ_f values is depicted in Fig. 3(a). All the cases show that the area of the injected Na_2SO_4 solution (plots) was larger than the area calculated from the injection volume (lines). The area $A_{\text{inj}}(t)$ calculated from the injection is defined as $A_{\text{inj}}(t) = qt/b$. The time evolution of the area difference for various τ_f values is depicted in Fig. 3(b). This figure shows the exponent value and the constant value of the power law scaling, $\Delta A = A_0 t^\alpha$, where A_0 is a constant of proportionality. We found that α was close to 2 at the highest τ_f , indicating that the area increase was primarily convection driven. This means that spontaneous convection driven by the spinodal decomposition sufficiently occurs and we can mention that sufficient spinodal decomposition occurred at the interfacial region. The exponent value decreased with decreasing τ_f and was close to 1 at the lowest τ_f . The results demonstrate that the interfacial phase separation was arrested by a decrease in τ_f (an increase in q). We note that a curve going as $t^{1.79}$ is growing slower than the linear growth because A_0 for $t^{1.79}$ growth (0.0168) is much smaller than A_0 for the linear growth (3.24).

Herein, we discuss the mechanism for the observed arrest of the interfacial phase separation. In the present flow configuration, wherein the two phase-separating solutions are nonpremixed and interact at the liquid-liquid interfacial region, a comparison between the flow rate and phase separation rate should be important. The previous paper [20] presented the result of interfacial

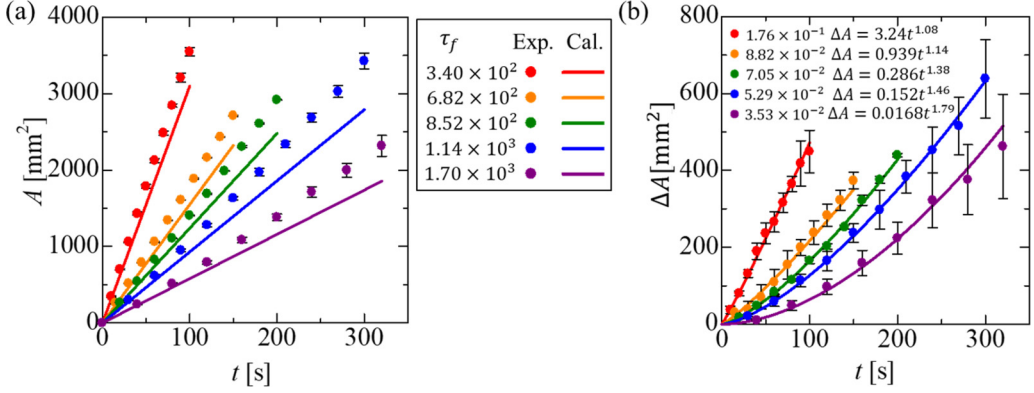


FIG. 3. (a) Measured area of injected 20 wt % Na_2SO_4 solution (plots) and area calculated from injection volume (lines) and (b) area difference between area of injected 20 wt % Na_2SO_4 solution and area calculated from injection volume for various τ_f . The plots and error bars represent the averages and standard deviations, respectively, for three or two experimental runs.

tension (γ) measurement between 36.5 wt % PEG and Na_2SO_4 solutions at various concentrations (12–20 wt %) using the spinning drop method. Notably, γ increased remarkably with time up to 50 s after contact of the PEG and Na_2SO_4 solutions and reached a constant value over 200–300 s [Fig. 6(a) in [20]]. The temporal increase in the interfacial tension is evidence of the occurrence of spinodal decomposition-type phase separation between the two fluids, which indicates a temporal increase in interfacial energy to generate force [20,30]. The force originating from the phase separation, called the Korteweg force, tends to minimize the free energy and can generate convection [20,21,26,31]. The Korteweg force is represented in terms of the free energy, as expressed in the following equation:

$$\mathbf{F}_i = \frac{\rho}{M_w} \frac{\delta G}{\delta \mathbf{r}} = \left(\frac{\rho RT}{M_w} \right) \mu_i \nabla \phi_i, \quad (1)$$

where ρ is the density, M_w is the molecular weight, \mathbf{r} is the position, and $\mu_i (= [\delta(G/RT)/\delta\phi_i])$ is the generalized chemical potential of component i , defined as the functional derivative of the molar Gibbs free energy of a nonuniform system for a ternary mixture. ϕ_i , R , and T represent the molar fraction, gas constant, and temperature. Three types of Korteweg forces exist in the ATPS. Among them, the Korteweg force generated by the interaction between water and PEG is the most dominant, constituting 96% or more of the total force [32]. Hence, the Korteweg force acts towards the outer PEG-rich phase, promoting droplet formation and increasing the area. The rate of increase in interfacial tension (γ) can be considered as a parameter representing the strength of the Korteweg force. The temporal evolution of γ can be fitted by the following equation: $\gamma = (\gamma_0 - \gamma_\infty)e^{-kt} + \gamma_\infty$, where γ_0 and γ_∞ are the values of γ at the contact time and at a time where γ becomes constant, respectively; this shows that the rate constant k increases with the concentration of Na_2SO_4 [Fig. 6(b) in [20]]. The rate constant k is also an indicator of the rate of phase separation occurring in the liquid-liquid interfacial region because the influence of convection is negligible in the spinning drop method.

In the present study, we first investigated how the exponent α , which appears in the expression of the power law of area growth of $\Delta A \propto t^\alpha$, is affected by the rate constant k . To do so, we performed the displacement experiments at the highest τ_f by varying the concentration of Na_2SO_4 , and we obtained the exponent α using the above-mentioned procedure. The results described in Fig. 4 show that α increases with k , indicating that the effect of the interfacial phase separation becomes stronger as the phase separation becomes faster for a fixed flow rate.

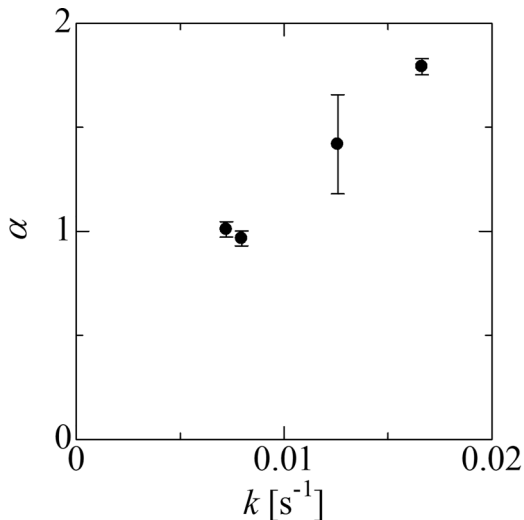


FIG. 4. Relationship between exponent α and rate constant k . The plots and error bars represent the averages and standard deviations, respectively, for three or two experimental runs.

We define the characteristic time of phase separation as the reciprocal of k , i.e., $\tau_p = 1/k$. We introduce a dimensionless number, defined as the ratio of the characteristic time of the flow (τ_f) to the characteristic time of the phase separation (τ_p), to compare the phase separation rate against flow rates; this number is expressed as τ_f/τ_p . When the flow rate is larger or the phase separation rate is smaller, the dimensionless number τ_f/τ_p becomes smaller. This dimensionless number corresponds to the Damköhler number used in fluid dynamics with chemical reaction to compare chemical reaction rates with flow rates [33,34]. The relationship between the exponent value α and reciprocal of τ_f/τ_p ($= \tau_p/\tau_f$) is depicted in Fig. 5 for various values of τ_f and k (the concentration of Na_2SO_4), where α can be expressed as a function of τ_p/τ_f on a single curve and monotonically decreases with an increase in τ_p/τ_f . The results systematically confirm that the competition between the imposed flow and phase separation rates determines the degree of phase separation occurring in the liquid-liquid interfacial region, and the interfacial phase separation is arrested by an increase in the reciprocal of the dimensionless number τ_f/τ_p ($= \tau_p/\tau_f$), which represents the phase separation rate against flow rates.

III. NUMERICAL SIMULATION

In the previous section, it is experimentally shown that the ratio of the imposed flow rate to the phase separation rates determines the degree of phase separation occurring in the liquid-liquid interfacial region, and the interfacial phase separation is arrested by an increase in the reciprocal of the dimensionless number representing the phase separation rate against flow rates. In the present section, we verify the mechanism by a numerical simulation.

As mentioned in Introduction, we succeeded in reproducing multiple droplets formation in VF with interfacial phase separation by a numerical simulation [27]. The VF with the interfacial phase separation involving Korteweg force can be described by three coupled equations; the continuum equation, Darcy's law [35,36] with the addition of a body force generated, i.e., Korteweg force, by the gradient of the chemical potential [21,37], and the modified Cahn-Hilliard equation to allow for transport dynamics of chemical species governing liquid-liquid phase separation [38]. In the aqueous two-phase system used, the viscosity and state of liquid phases are determined by the concentration of PEG [32]. Furthermore, the Korteweg force is contributed largely by the interaction between PEG and water [24–26,32]. The dynamics of one species (here, PEG) allows

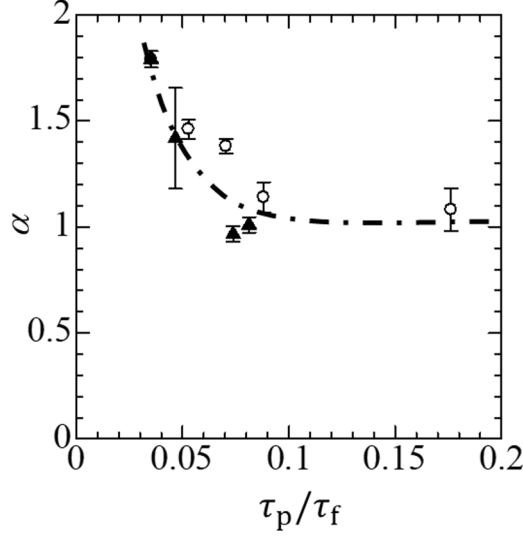


FIG. 5. Relationship between exponent α and τ_p/τ_f . The plots and error bars represent the averages and standard deviations, respectively, for three or two experimental runs. The open plots represent values corresponding to varying τ_f at fixed τ_p , whereas triangle plots represent values corresponding to varying τ_p at fixed τ_f .

us to understand the thermodynamic state and hydrodynamic properties of each phase. Thus, the nondimensional governing equations in a moving reference frame in the previous simulation [27] are as follows:

$$\nabla \cdot \mathbf{u} = 0, \quad (2)$$

$$\nabla P = -\eta(c)(\mathbf{u} + \mathbf{i}) + \delta[\mu(c, p)\nabla c], \quad (3)$$

$$\frac{\partial c}{\partial t} + \mathbf{u} \cdot \nabla c = \frac{1}{\text{Pe}} \nabla^2 \mu(c, p), \quad (4)$$

$$\mu(c, p) = \frac{\delta f(c, p)}{\delta c} = -\alpha_1 \nabla^2 c - \alpha_2 (c - p) + \alpha_3 (c - p)^3, \quad (5)$$

$$\eta(c) = e^{Rc}, \quad (6)$$

$$f(c, p) = -\frac{\alpha_2}{2}(c - p)^2 + \frac{\alpha_3}{4}(c - p)^4, \quad (7)$$

where \mathbf{u} is the velocity, P is the hydrodynamic pressure, c is the concentration of the one species, $\eta(c)$ is the viscosity, \mathbf{i} is the unit vector in the x direction, α_1 implies the interfacial energy such as interfacial tension, α_2 and α_3 are the transport coefficients such as diffusion and phase separation, δ is the coefficient of the Korteweg force, $R = \ln[\eta(c = c_1)/\eta_0]$ is the log-mobility ratio, $f(c, p)$ is a free energy of the bulk phase, and $\mu(c, p)$ is the chemical potential, which is a functional derivative of the free energy with respect to concentration. Here, the Péclet number, $\text{Pe} = UL_y/M = \tau_D/\tau_F$, for the simulation is the ratio of the diffusive time, $\tau_D = L_y^2/M$, and the advective time, $\tau_F = L_y/U$, where U is the injection velocity, L_y is the length scale, and M is a phenomenological mobility coefficient during phase separation, which can be inferred from mutual diffusion and phase separation. In the present study, τ_D is considered to be compatible with τ_p (the characteristic time of phase separation). This is because larger diffusivity for phase separation implies a larger rate of phase separation. Therefore, Pe represents the nondimensional number showing the ratio of the imposed flow rate and the phase separation rate. Note that the numerical

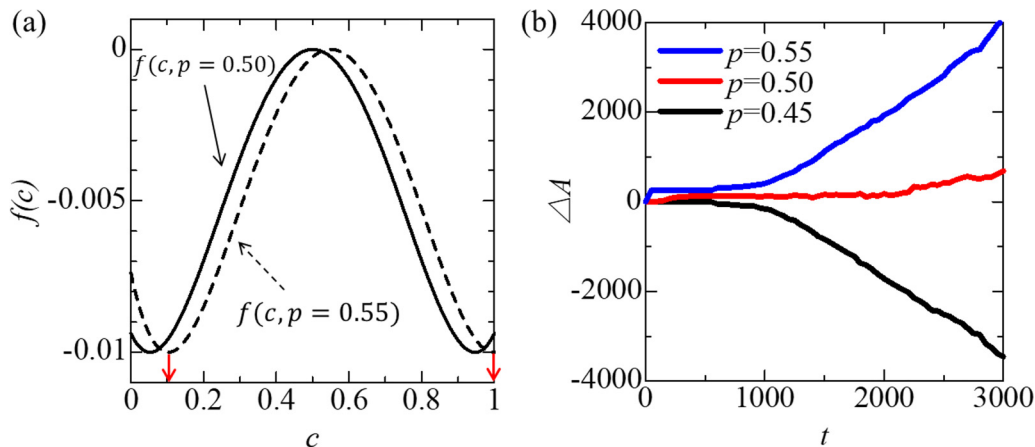


FIG. 6. (a) Free energy $f(c, p = 0.50)$ and translated free energy $f(c, p = 0.55)$ and (b) area difference for various parameter p . The red arrows in (a) represent the equilibrium concentrations for $f(c, p = 0.55)$. The equilibrium concentrations are $c = 0.103$ and $c = 0.997$.

simulation using the above equations demonstrates that the multiple droplet pattern instead of the fingering pattern formed with the increase in the effect of phase separation [27] at fixed Pe . In this study, we change Pe to numerically investigate the effect of the imposed flow on VF dynamics and to theoretically verify the interfacial phase separation arrested by the imposed flow and its proposed mechanism.

A change in volume ratio of the separated solutions is also important to mimic the experiment because two solutions with equal volume are mixed with each other and then the volume ratio of the separated solutions is not 1 in the experiment. Namely, when 100 mL of 36.5 wt % PEG solution and 100 mL of 20 wt % Na_2SO_4 solution are mixed, the mixed solution separates into about 97 mL of PEG-rich phase and about 103 mL of salt-rich phase. The parameter p in Eq. (7) is used to change the volume ratio of both phases after phase separation to mimic the experiment [Fig. 6(a)]. The lever rule determines the mass ratio, i.e., volume ratio, of each phase after phase separation. If the initial concentration exists at the center of the tie line in the phase diagram, the volume ratios of the two phases after phase separation will be equal. If the initial concentration is off center, however, the volume of the two phases after phase separation will be asymmetric according to the lever rule. In this numerical simulation, the volume change after phase separation can be produced by translating the free energy in the horizontal direction. The free energy can be shifted horizontally by changing the value of the parameter p in Eq. (7), which corresponds to the change in equilibrium concentrations [Fig. 6(a)]. In the simulation, the initial concentration at the interface where the instability occurs is fixed at a constant of $c = 0.5$. A horizontal shift in free energy corresponds to the change in the equilibrium concentration on the tie line of the phase diagram. Figure 6(b) shows the effect of the p value on the area difference ΔA , which is calculated from the injected area subtracted from the area occupied by the displacing fluid for a condition employed in Fig. 7, that is, three different p and $Pe = 2$, $R = 0.5$, $\alpha_1 = 1$, $\alpha_2 = 0.2$, $\alpha_3 = 1$, $\delta = 100$. The area difference ΔA is almost constant against time when $p = 0.5$, whose condition is the same as the case reported by Seya *et al.* [27]. The area increase is observable at $p = 0.55$ and the area decrease can be seen at $p = 0.45$. This reason is explained by using the free energy and initial condition. Since the initial concentration at the interface is $c = 0.5$ and the equilibrium concentrations are $c = 0.053$ and $c = 0.947$ based on the free energy $f(c, p = 0.5)$ [Fig. 6(a)], the volume ratio of the displacing less viscous solution and the displaced more viscous solution is $\frac{0.947-0.5}{0.5-0.053} = 1.0$. Here, the numerator is the length of the tie line of the more viscous solution side, while the denominator is one of the less viscous solution side. Under the lever rule, the volume ratio after phase separation becomes

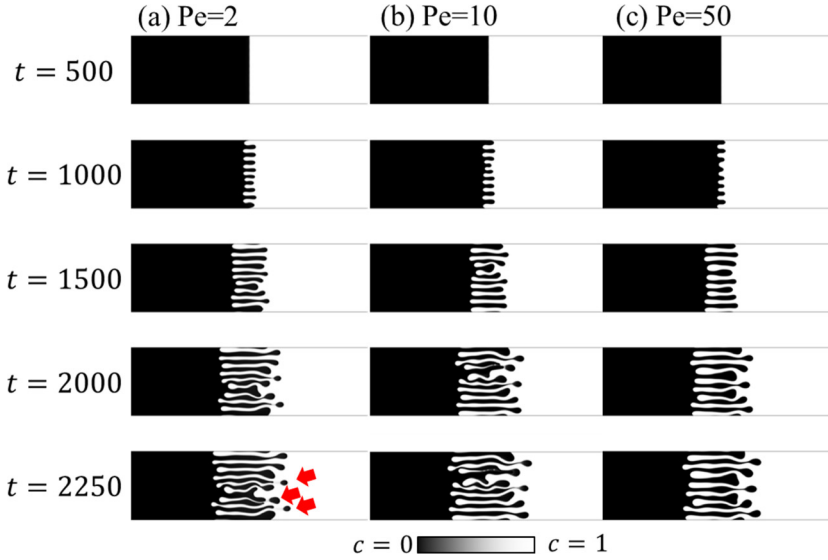


FIG. 7. Time evolution of displacement patterns at (a) $Pe = 2$, (b) $Pe = 10$, and (c) $Pe = 50$ for the numerical simulation ($R = 0.5$, $\alpha_1 = 1$, $\alpha_2 = 0.2$, $\alpha_3 = 1$, $\delta = 100$, $p = 0.55$). The red arrows show the droplets.

the inverse ratio of the length of the tie line. Therefore, the decimal fraction ($\frac{0.947-0.5}{0.5-0.053} = 1.0$) means the volume ratio of the displacing less viscous solution and the displaced more viscous solution after phase separation. Under the condition of $p = 0.55$ indicating that the equilibrium concentrations are $c = 0.103$ and $c = 0.997$ based on the free energy $f(c, p = 0.55)$ [Fig. 6(a)], the volume ratio is $\frac{0.997-0.5}{0.5-0.103} = 1.25$, which means the area of the displacing less viscous solution increases in the simulation. Here again, the numerator is the length of the tie line of the more viscous solution side, while the denominator is one of the less viscous solution side. Since the volume ratio after phase separation becomes the inverse ratio of the length of the tie line under the lever rule, the decimal fraction ($\frac{0.997-0.5}{0.5-0.103} = 1.25$) means the volume ratio of the displacing less viscous solution and the displaced more viscous solution after phase separation. We employed $p = 0.55$ in the present study as a representative example of $p > 0.5$ because the phase separation increases the volume of the less viscous (displacing) liquids in the experiment. We note that $p = 0.45$ is used as a representative example of $p < 0.5$ where the phase separation decreases the volume of the less viscous (displacing) liquids.

Figure 7 shows the temporal evolution of VF with phase separation for various Pe in the numerical simulation results. The time progresses in the down direction and Pe becomes larger with the right direction. At $t = 500$, no fluctuation occurs for any Pe cases. A fingering pattern occurs for any Pe cases at $t = 1000$. For low Pe ($Pe = 2$), droplets are observed at $t = 2250$. Red arrows highlight the formation of the droplets. For high Pe ($Pe = 50$), however, no droplets are observed even at $t = 2250$. Thus, the numerical calculations show that no droplets form and the viscous fingers become somewhat thicker as Pe increases. This observation is like that obtained in experiments when the flow rate is increased. This indicates that the degree of the interfacial phase separation on VF is shown numerically to be determined by the ratio between the imposed flow rate and the phase separation rate.

The time evolution of the area difference for various Pe is depicted in Fig. 8. The simulation result (Fig. 8) shows the same trend as Fig. 3(b). Note that the time t' defined as $t \times u/U$ is used to compare with the experimental results.

Figure 9 shows the relationship between Pe and the growth exponent α calculated from $\Delta A \propto t^\alpha$ for the numerical simulation. We find that arresting effects similar to those obtained in experiments

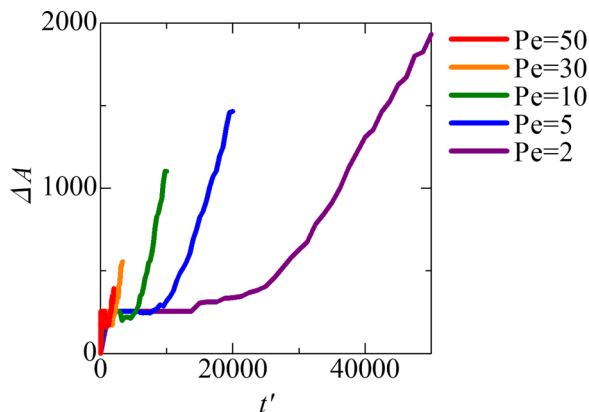


FIG. 8. Time evolution of area difference for the numerical simulation for various Pe . t' in the simulation indicates a normalized time, $t \times \frac{\mu}{\sigma}$, to compare with the experimental results in Fig. 3.

can be obtained in the numerical simulation. This numerical result shows that the competition between the imposed flow and phase separation rates is numerically shown to determine the degree of interfacial phase separation. We note that quantitative comparison between the value of Pe and τ_p/τ_f is not feasible due to the difference of the definition. Based on the results, where the droplet formation is observed at low Pe or τ_p/τ_f and the exponent α decreases from 2 to 1 as Pe or τ_p/τ_f increases in both experiments and numerical simulations, the influence of Pe in the numerical simulations and the influence of τ_p/τ_f in the experiments is considered to be same.

Here, we highlight the link between the experiments and numerical simulation, where we focus on the necessity of using different dimensionless groups for the experiments and simulations. In the experiments, we calculated the phase separation rate or the characteristic time of phase separation from the increasing rate of interfacial tension, which can be measured by experiments. Also, the characteristic time of flow is calculated from the residence time in the Hele-Shaw cell. We compare phase separation rate with flow rate by using these characteristics times of phase separation and flow. On the other hand, by considering the phase separation rate as the diffusive rate for phase separation

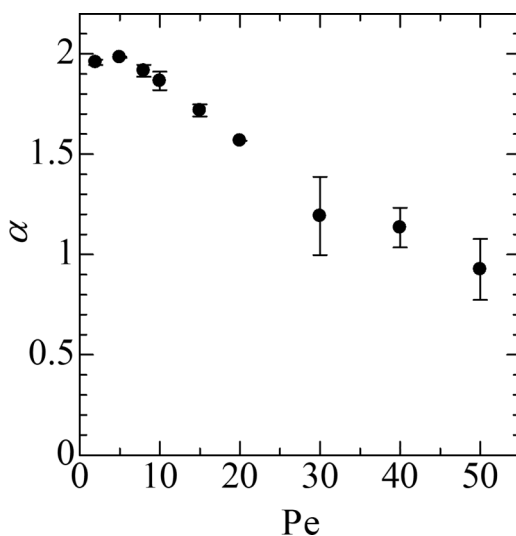


FIG. 9. Relationship between α and Pe for the numerical simulation. The plots and error bars represent the averages and standard deviations, respectively, for three or two numerical runs.

in the numerical simulations, we investigate the influence of the ratio of phase separation rate and flow rate by using the ratio of diffusive rate and flow rate, i.e., Pe , which appears in the mathematical modeling developed by Seya *et al.* [27]. Therefore, the meaning of Pe in the numerical simulation is the same as the meaning of τ_p/τ_f in the experiment.

We emphasize that the mechanism for the interfacial phase separation arrest in the present study is different from that occurring in the bulk phase, especially in turbulent flows, which has been reported by previous studies. Regarding the arrest in turbulent flows, it has been shown that the intensity of turbulence (which twists, folds, and breaks interfaces into smaller domains) determines the degree of coarsening (which leads to domain growth) arrest, and a stronger arrest is achieved by a larger turbulent intensity [15]. The phase separation in our system is limited to the vicinity of the interface because only the interface where diffusion is occurring falls into the spinodal region. Hydrodynamic instability is also limited to the vicinity of the interface because it originates from the viscosity contrast between the two phases in the interface.

IV. CONCLUSION

In conclusion, we experimentally investigated the displacement of a more viscous liquid by a less viscous liquid in Hele-Shaw cells using an ATPS; such a displacement can cause phase separation in the growing liquid-liquid interfacial region by varying the flow rate and the phase separation rate. We evaluated the degree of the interfacial phase separation during fluid displacement using the temporal evolution of the increase in area of the displacing liquid caused by the phase separation, in the form $\Delta A \sim t^\alpha$. Our results show that the exponent α is close to 2 at the highest τ_f (lowest q), and decreases monotonically with a decrease in τ_f (an increase in q). This indicates that the area increase is convection-driven for a higher τ_f (lower q) and suppressed by a decrease in τ_f (an increase in q). Therefore, it can be concluded that the interfacial phase separation is arrested by an increase in the flow rate, because spontaneous convection is originated from the phase separation. We demonstrated that the competition between the flow rate and phase separation rate determines the degree of phase separation occurring in the liquid-liquid interfacial region by introducing the dimensionless number τ_p/τ_f , which represents the phase separation rate against flow rates. The same arresting effect as that observed in the experiment was obtained by the numerical calculation with varying Pe . In the simulation, Pe represents the ratio of the imposed flow rate and the phase separation rate because characteristic time of diffusion for the phase separation is considered to be compatible with the characteristic time of phase separation. Therefore, the numerical results theoretically demonstrate the mechanism that the competition between the flow rate and phase separation rate determines the degree of phase separation occurring in the liquid-liquid interfacial region. We describe that the mechanism for the interfacial phase separation arrest in the present study is different from that occurring in the bulk phase.

Phase separation arrests due to imposed flows have been reported in various flow fields, such as simple shear flows, 2D and 3D turbulent flows, and chaotic flows. In all previous studies, phase separation occurred in the bulk phase. This study demonstrates an imposed flow-arresting phase separation occurring at a growing liquid-liquid interfacial region. The present study will lead to research trends focusing on the coupling between phase separation and hydrodynamics, especially phase separation arrests caused by imposed flows. In addition, the subject treated here, i.e., phase separation occurring at a growing liquid-liquid interfacial region arrested by an imposed flow, is highly relevant to a methodology for the control of interfacial hydrodynamics by phase separation [30], which will be useful for optimization of processes in various fields, from enhanced oil recovery [39], CO₂ sequestration [40], and treatment of oil slicks on the surface of the ocean [41–43] on a large scale to microfluidic devices [44,45] on a small scale in engineering fields. Furthermore, the concept of phase separation being arrested by an imposed flow in a liquid-liquid interfacial region could provide a more comprehensive understanding of cell biology because droplet formation occurs owing to a possible phase separation of different proteins in the liquid-liquid interfacial region in a living cell [46].

ACKNOWLEDGMENTS

We acknowledge financial support of JSPS KAKENHI Grants No. 19K04189, No. 22K03900, and No. 22K20402 and JST PRESTO Grant No. JPMJPR22O5. M.M. was also supported by JSPS Invitation Fellowships for Research in Japan (Grant No. L 19548). The authors thank Editage [47] for English language editing.

-
- [1] J. S. Huang, S. Vernon, and N. C. Wong, Homogeneous nucleation in a critical binary fluid mixture, *Phys. Rev. Lett.* **33**, 140 (1974).
 - [2] E. D. Siggia, Late stages of spinodal decomposition in binary mixtures, *Phys. Rev. A* **20**, 595 (1979).
 - [3] D. A. Porter, K. E. Easterling, and M. Sherif, *Phase Transformations in Metals and Alloys*, 3rd ed. (CRC, Boca Raton, 2009).
 - [4] P. W. Voorhees, Ostwald ripening of two-phase mixtures, *Annu. Rev. Mater. Sci.* **22**, 197 (1992).
 - [5] I. M. Lifshitz and V. V. Slyozov, The kinetics of precipitation from supersaturated solid solutions, *J. Phys. Chem. Solids* **19**, 35 (1961).
 - [6] C. Wagner, Theorie der alterung von niederschlägen durch umlösen (Ostwald-Reifung), *Z. Elektrochem., Ber. Bunsengesellschaft Phys. Chem.* **65**, 581 (1961).
 - [7] K. Y. Min and W. I. Goldburg, Nucleation of a binary liquid mixture under steady-state shear, *Phys. Rev. Lett.* **70**, 469 (1993).
 - [8] T. Hashimoto, K. Matsuzaka, E. Moses, and A. Onuki, String phase in phase-separating fluids under shear flow, *Phys. Rev. Lett.* **74**, 126 (1995).
 - [9] A. Onuki, Phase transitions of fluids in shear flow, *J. Phys.: Condens. Matter* **9**, 6119 (1997).
 - [10] Z. Shou and A. Chakrabarti, Ordering of viscous liquid mixtures under a steady shear flow, *Phys. Rev. E* **61**, R2200 (2000).
 - [11] C. C. Chueh, A. Bertei, and R. Mauri, Dynamics of phase separation of sheared inertialess binary mixtures, *Phys. Fluids* **32**, 023307 (2020).
 - [12] D. J. Pine, N. Easwar, J. V. Maher, and W. I. Goldburg, Turbulent suppression of spinodal decomposition, *Phys. Rev. A* **29**, 308 (1984).
 - [13] P. Tong, W. I. Goldburg, J. Stavans, and A. Onuki, Temporal fluctuations in a turbulently stirred binary liquid mixture, *Phys. Rev. Lett.* **62**, 2668 (1989).
 - [14] S. Berti, G. Boffetta, M. Cencini, and A. Vulpiani, Turbulence and coarsening in active and passive binary mixtures, *Phys. Rev. Lett.* **95**, 224501 (2005).
 - [15] P. Perlekar, R. Benzi, H. J. H. Clercx, D. R. Nelson, and F. Toschi, Spinodal decomposition in homogeneous and isotropic turbulence, *Phys. Rev. Lett.* **112**, 014502 (2014).
 - [16] P. Perlekar, N. Pal, and R. Pandit, Two-dimensional turbulence in symmetric binary-fluid mixtures: Coarsening arrest by the inverse cascade, *Sci. Rep.* **7**, 44589 (2017).
 - [17] L. Berthier, J.-L. Barrat, and J. Kurchan, Phase separation in a chaotic flow, *Phys. Rev. Lett.* **86**, 2014 (2001).
 - [18] X. Fu, L. Cueto-Felgueroso, and R. Juanes, Thermodynamic coarsening arrested by viscous fingering in partially miscible binary mixtures, *Phys. Rev. E* **94**, 033111 (2016).
 - [19] G. M. Homsy, Viscous fingering in porous media, *Annu. Rev. Fluid Mech.* **19**, 271 (1987).
 - [20] R. X. Suzuki, Y. Nagatsu, M. Mishra, and T. Ban, Phase separation effects on a partially miscible viscous fingering dynamics, *J. Fluid Mech.* **898**, A11 (2020).
 - [21] N. Vladimirova, A. Malagoli, and R. Mauri, Diffusiophoresis of two-dimensional liquid droplets in a phase-separating system, *Phys. Rev. E* **60**, 2037 (1999).
 - [22] D. Molin, R. Mauri, and V. Tricoli, Experimental evidence of the motion of a single out-of-equilibrium drop, *Langmuir* **23**, 7459 (2007).
 - [23] P. Poesio, G. P. Beretta, and T. Thorsen, Dissolution of a liquid microdroplet in a nonideal liquid-liquid mixture far from thermodynamic equilibrium, *Phys. Rev. Lett.* **103**, 064501 (2009).

- [24] T. Ban, A. Aoyama, and T. Matsumoto, Self-generated motion of droplets induced by Korteweg force, *Chem. Lett.* **39**, 1294 (2010).
- [25] T. Ban, T. Yamada, A. Aoyama, Y. Takagi, and Y. Okano, Composition-dependent shape changes of self-propelled droplets in a phase-separating system, *Soft Matter* **8**, 3908 (2012).
- [26] T. Ban, T. Fukuyama, S. Makino, E. Nawa, and Y. Nagatsu, Self-propelled vesicles induced by the mixing of two polymeric aqueous solutions through a vesicle membrane far from equilibrium, *Langmuir* **32**, 2574 (2016).
- [27] S. Seya, R. X. Suzuki, Y. Nagatsu, T. Ban, and M. Mishra, Numerical study on topological change of viscous fingering induced by a phase separation with Korteweg force, *J. Fluid Mech.* **938**, A18 (2022).
- [28] S. M. Snyder, K. D. Cole, and D. C. Sziag, phase compositions, viscosities, and densities for aqueous two-phase systems composed of polyethylene glycol and various salts at 25 °C, *J. Chem. Eng. Data* **37**, 268 (1992).
- [29] See Supplemental Material at <http://link.aps.org/supplemental/10.1103/PhysRevFluids.9.024003> for movies of temporal pattern evolution for various τ_f values.
- [30] T. Ban, Y. Kobayashi, R. Suzuki, and Y. Nagatsu, Active liquid matter driven by nonequilibrium interfacial tension, *J. Phys. Soc. Jpn.* **86**, 101005 (2017).
- [31] K. Iwasaki, Y. Nagatsu, T. Ban, J. Iijima, M. Mishra, and R. X. Suzuki, Experimental demonstration of the suppression of viscous fingering in a partially miscible system, *Phys. Chem. Chem. Phys.* **25**, 13399 (2023).
- [32] R. X. Suzuki, Y. Nagatsu, M. Mishra, and T. Ban, Fingering pattern induced by spinodal decomposition in hydrodynamically stable displacement in a partially miscible system, *Phys. Rev. Fluids* **4**, 104005 (2019).
- [33] J. Fernandez and G. M. Homsy, Viscous fingering with chemical reaction: effect of in-situ production of surfactants, *J. Fluid Mech.* **480**, 267 (2003).
- [34] R. Tsuzuki, T. Ban, M. Fujimura, and Y. Nagatsu, Dual role of surfactant-producing reaction in immiscible viscous fingering evolution, *Phys. Fluids* **31**, 022102 (2019).
- [35] C. T. Tan and G. M. Homsy, Simulation of nonlinear viscous fingering in miscible displacement, *Phys. Fluids* **31**, 1330 (1988).
- [36] S. Pramanik and M. Mishra, Effect of Péclet number on miscible rectilinear displacement in a Hele-Shaw cell, *Phys. Rev. E* **91**, 033006 (2015).
- [37] D. Jasnow and J. Viñals, Coarse-grained description of thermo-capillary flow, *Phys. Fluids* **8**, 660 (1996).
- [38] J. W. Cahn and J. E. Hilliard, Free energy of a nonuniform system. I. Interfacial free energy, *J. Chem. Phys.* **28**, 258 (1958).
- [39] L. W. Lake, R. T. Johns, W. R. Rossen, and G. A. Pope, *Fundamentals of Enhanced Oil Recovery* (Society of Petroleum Engineers, Richardson, TX, 2014).
- [40] F. M. J. Orr and J. J. Taber, Use of carbon dioxide in enhanced oil recovery, *Science* **224**, 563 (1984).
- [41] M. Reed, O. Johansen, P. J. Brandvik, P. Daling, A. Lewis, R. Fiocco, D. Mackay, and R. Prentki, Oil spill modeling towards the close of the 20th century: overview of the state of the art, *Spill Sci. Technol. Bull.* **5**, 3 (1999).
- [42] S. D. Wang, Y. M. Shen, and Y. H. Zheng, Two-dimensional numerical simulation for transport and fate of oil spills in seas, *Ocean Eng.* **32**, 1556 (2005).
- [43] M. J. Olascoaga and G. Haller, Forecasting sudden changes in environmental pollution patterns, *Proc. Natl. Acad. Sci. USA* **109**, 4738 (2012).
- [44] H. A. Stone, A. D. Stroock, and A. Ajdari, Engineering flows in small devices, *Annu. Rev. Fluid Mech.* **36**, 381 (2004).
- [45] G. M. Whitesides, The origins and the future of microfluidics, *Nature (London)* **442**, 368 (2006).
- [46] E. Dolgin, Cell biology's new phase, *Nature (London)* **555**, 300 (2018).
- [47] www.editage.com.